

### response to associate editor

We hope that your first point—concerning considering a dataset with non-Gaussian residuals—is covered appropriately under the “Main Issue” in the response to the additional review by reviewer 4 below. As stated there, the point of using SPINE is not to defend against serious outliers but to extend the range of reliable age determination beyond that possible with YORK

- 5 In fact, we have performed model 3 calculations on sample 0708, and also on some simulated datasets. The results are interesting, but they make it seem unwise for us to include model 3 calculations in Appendix A. Our first concern is that we don’t think it is appropriate to consider the scatter that is to be handled by geological variation to start at  $m_{swd} = 1$ . In the case of sample 0708, data scatter is consistent with analytical uncertainties for  $m_{swd} < 1.2$ , at 95% confidence. Doesn’t using  $m_{swd} = 1$  to flag the necessity of including geological variation potentially overestimate the variation?
- 10 The second concern does not show for sample 0708 because the distribution of the residuals is close to Gaussian, although far enough away from Gaussian that  $m_{swd}$  “fails”. One consequence is that YORK and SPINE give very similar ages. But, in general, it seems that the age determined with model 3 is insensitive to the geological variation, however the age is determined. Thus, if the data structure means that YORK has functioned sub-optimally because of outliers, a model 3 calculation performed using YORK (as done in isoplot) may give a rather different result to the same calculation done using SPINE. Such outliers may
- 15 well be a valid part of the geological variation, so they are not in fact outliers in the context of model 3. Generally, then, won’t using YORK for model 3 calculations potentially result in overestimated geological variation, as well as an unreliable age?
- The changes to the manuscript are indicated in the response to the additional review, and are in blue in the revised version below.

### response to additional review of reviewer 4

- 20 The additional comments by reviewer 4 are much appreciated. Before responding to these, a left-over matter from this reviewer’s first review, is the observation that the iteration used to find  $\theta$ —the parameters of the best-fit line—is likely to be unreliable in general. We asserted that attempts to find an iteratively reweighted least squares iteration had failed, and indeed that all the simulations undertaken had been successful with the iteration given. Nevertheless, following submission of the revision, the first author tried again, and has indeed derived an iteratively reweighted least squares iteration (based on Maronna
- 25 *et al.*, 2019, Section 4.5.2, but including the analytical uncertainties). This is now adopted in the python code in Appendix C as a more reliable (and also more concise) approach. The logic of the original iteration is still retained in Appendix B as it is necessary for the derivation of the covariance matrix of  $\theta$ .

### Small issues:

- 30 1. While we hope to retain the term “excess scatter” as a short-hand way of referring to the consequence of fat tails, a form of words based on the reviewer’s commentary is now given in a footnote (following the suggestion of using footnotes by the reviewer in his point 7), to clarify this usage.
2. It is quite correct that the spine width,  $s$  (or, strictly,  $\hat{s}$ ) says nothing about whether the centre of the distribution of  $r$  is Gaussian or not. The wording related to this has been tightened up.
- 35 3. If all the  $|r_k| \leq h$  in a dataset, then SPINE results are literally identical to YORK and  $\sum \rho(r_k)$  does equal  $(n - 2)m_{swd}$  then. For example, for  $n = 10$ , some 17% of strictly Gaussian-distributed data have datasets with no  $|r_k| > h$ . Otherwise the reviewer is correct that SPINE results are only nearly identical to YORK results for “good” datasets. This has been clarified in the text.
4. In using the word “resistant”, we were following Huber & Rochetti (2009, Sect 1.2.3), though now we see that Maronna *et al.* (2019) does not use the resistant–robust distinction. Resistant is no longer used in the manuscript.
- 40 5. Good idea: Tukey reference added.
6. The term “Tera-Wasserburg” has now been deleted. It is unnecessary here—it just refers to this particular type of isotope plot.

7. A footnote has been added relating to the `nmad` normalisation.

8. While we understood that using circumflex on estimators is strictly correct, we are hoping to forgo that for the sake of keeping the notation less cluttered, and for the main audience of our paper.

#### Moderate issues:

1. Some confusion in the mind of the first author regarding efficiency has now been dispelled. The words relating to efficiency should now be appropriate.

2. Agreed, robust data fitting methods are good, and can be applied to datasets that are more scattered than those usually encountered in geochronology. The problem is that in geochronology there is an expectation of a statistical test that suggests whether a dataset has age significance (isochron) or not (errorchron). For example, in the covering letter from the associate editor requesting us to submit a revision, in which he asked how do we stop the “rubbish in–rubbish out” problem in data fitting (which we took to mean an errant dataset giving an age that is geologically meaningless). So we do make a distinction—akin to the one based on `mswd`—via the information in Table 1. This is a rabbit hole—but unfortunately one that we have been forced down. We accept that the good behaviour of SPINE makes such a decision unnecessary. But the `mswd` limit was less to prevent the potentially-errant behaviour of YORK (mostly not acknowledged, or even ignored), and more to do with assessing whether a dataset gives a geological meaningful age (deemed to be when the data were consistent with strictly Gaussian-distributed data).

3. The use of `mswd`, rather than  $R^2$ , seems to be a historical accident in geochronology going back at least to the early York and other papers in the mid-60s. We don’t know why  $R^2$  was never adopted. Certainly  $R^2$  is not given by ISOPLOT.

4. Yes. Whereas it is currently asserted in the manuscript that `nmad(r)` somehow discerns whether the central part of the distribution of `r` is effectively Gaussian, in fact this is plainly not correct. The spine width cannot do that. In the context that it is used, all that is required of the spine width is that it reflects the presence of a spine in the data. Nothing more. The wording in the manuscript has been modified to reflect this. It is not necessary to show that the central part of the distribution of the residuals is Gaussian for SPINE to work, and, as the reviewer points out, the central part of the distribution will tend to be approximately Gaussian anyway.

#### Main issue:

The usual demonstration of the deleterious effect of outliers on least squares (equivalently, YORK) uses datasets with very obvious outliers, e.g. Maronna *et al.* (2019), Fig. 4.3. Particularly in geochronology, such datasets would not be used in data-fitting for age determination. If used, they may well “cleaned up” first (but with the problems that can arise from that, as discussed in the robust statistics literature). Nevertheless, as expected, SPINE does work well in the presence of egregious outliers, finding the main trend of the data.

The purpose of using SPINE is not handling obvious outliers, rather the purpose is to extend the range of datasets for which a reliable age can be determined, where the deleterious effect of data scatter is real, but not dramatic as it is in the Maronna example. This effect can be seen clearly in new simulations, using for example residuals distributed as 10%10N with  $n = 10$ . For 10,000 simulated datasets, with a nominal age of 4 Ma, for the datasets that “fail” `mswd`, a 95% confidence interval on the SPINE age is  $4 \pm 0.033$  Ma, whereas for YORK it is  $4 \pm 0.092$  Ma. Also, the age difference between the two methods, normalised by the  $\sigma$  on the SPINE age, is  $\pm 5.54$ . Such calculations showing the reliability of SPINE, beyond the range of data scatter that YORK can handle, are now summarised in Section 2.4.

It is not clear that what the reviewer wants to see in a graphical demonstration of the success of SPINE is actually easy to achieve with a geochronologically-available or -sensible dataset. Instead, we show this via a simulated dataset in Appendix E in the revision, also using a quantile-quantile plot, hoping that they might be used more widely in this context.

# Robust Isochron Calculation

Roger Powell<sup>1</sup>, Eleanor CR Green<sup>1</sup>, Estephany Marillo Sialer<sup>1</sup>, and Jon Woodhead<sup>1</sup>

<sup>1</sup>School Earth Sciences, The University of Melbourne, Vic 3010, Australia

**Correspondence:** Roger Powell (powell@unimelb.edu.au)

## Abstract.

The standard classical statistics approach to isochron calculation assumes that the distribution of uncertainties on the data arising from isotopic analysis is strictly Gaussian. This effectively excludes from consideration datasets that have excess scatter, even though many appear to have age significance. A new approach to isochron calculations is developed in order to circumvent this problem requiring only that the central part of the uncertainty distribution of the data defines a “spine” in the trend of the data. [This central spine can be Gaussian but this is not a requirement.](#) This approach significantly increases the range of datasets from which age information can be extracted but also provides seamless integration with well-behaved datasets, and thus all legacy age determinations. A statistical test is provided to ascertain that there is a spine in the data. Then a robust line-fitting approach is adopted that is more reliable when used on data with excess scatter but is coincident with the classical statistics approach for datasets without excess scatter. A calculation method for the algorithm is presented, accompanied by an implementation in Python.

## 1 Introduction

The ability to fit a straight line through a body of isotope ratio data in order to form an isochron is the cornerstone of many geochronological methods. In detail, however, this is a non-trivial task, since uncertainties are usually associated with all variables, and these are often correlated, precluding simple “least squares” line-fitting techniques. Most of the research in this area was conducted in the late 1960’s and early 1970’s, being dominated by a classical statistics approach in which data uncertainties, derived from the analytical methods, are taken to be strictly Gaussian-distributed (e.g. York, 1969; York et al., 2004, and references therein). This approach, referred to here as YORK, became entrenched in the geochemical community, particularly in the last two decades as the essential component of the very widely-used software, ISOPLOT, e.g. Ludwig (2012).

In this contribution we examine some of the problems inherent in these techniques and suggest an alternative approach. Our primary focus here will be on general-purpose isochron calculations that determine the age of an “event” that established the isotopic compositions of samples in a dataset. This involves what are called model 1 and 2 calculations in ISOPLOT - as described below. Approaches that try to extract detail within events, including ISOPLOT model 3 calculations, are not considered (but see e.g. Vermeesch, 2018).

## 1.1 On ISOPLOT

In order to show that there are significant problems in using ISOPLOT for general-purpose isochron calculations, and then to see how they can be addressed, it is first necessary to outline the ISOPLOT protocol, some details of which may not be apparent to the end user. Central to the ISOPLOT workflow, the main tool for considering data scatter is  $m_{swd}$ , the mean standard weighted deviates (also called the reduced chi-squared statistic), see eq. 1. For strictly Gaussian distributed uncertainties  $(n-2)m_{swd}$  is distributed as chi-squared ( $\chi_{n-2}^2$ ), meaning that if uncertainties are correctly assigned, a strong statistical statement can be made about whether the scatter of a particular dataset is solely consistent with the associated data uncertainties (i.e. with no geological scatter), for example in the form of a 95% confidence interval on  $m_{swd}$ , Wendt and Carl (1991). Such a confidence interval is not fixed, but depends on the number of datapoints under consideration, so for example for  $n = 10$ ,  $m_{swd} < 1.94$  (meaning that  $m_{swd}$  extends from less than 1 through to 1.94), while for  $n = 50$ ,  $m_{swd} < 1.36$ . A dataset with  $m_{swd}$  in the chosen range for the number of datapoints has data scatter that is consistent with the data uncertainties. This situation is commonly referred to as  $m_{swd}$  “passes”; otherwise  $m_{swd}$  “fails”, in relation to  $\chi_{n-2}^2$ . The situation where  $m_{swd}$  passes provides a “pure” interpretation of YORK, and, in ISOPLOT is referred to as a model 1 isochron fit. This is depicted as the horizontal line in Fig. 1, indicating that in this range of  $m_{swd}$ , corresponding to a confidence interval, the calculated uncertainty on an isochron age does not vary with  $m_{swd}$ . Such a figure is drawn by taking an actual dataset and progressively modifying it to show what happens as  $m_{swd}$  varies, as described in Appendix A.

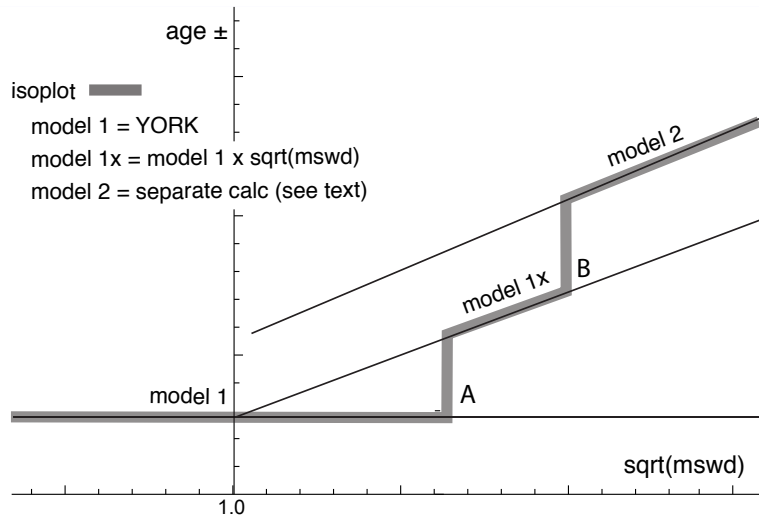


**Figure 1.** Age uncertainty ( $age \pm$ ) plotted against  $\sqrt{m_{swd}}$  under the ISOPLOT protocol for a progressively modified dataset (see text, and Appendix A). Under the condition of a model 1 fit, the age uncertainty is constant with increasing data scatter (reflected in increasing  $m_{swd}$ ), until there is a step change in the data treatment at A when the age uncertainty is multiplied by  $\sqrt{m_{swd}}$ . Then at B there is another step change in age uncertainty calculation with increasing data scatter forming ISOPLOT model 2 (see text)

What if  $m_{swd}$  is greater than the upper limit of the chosen confidence interval? Then the data are considered to have *excess* scatter, in addition to that accounted for by the data uncertainties (assuming that they are strictly Gaussian)<sup>1</sup>. At this point, 125 ISOPLOT, asks the user whether an alternative—model 2—calculation should be undertaken. This decision point is indicated at A in Fig. 1. If the user declines, ISOPLOT gives results that are referred to here as model 1x, as shown in Fig. 1. The model 1 age uncertainty is multiplied by  $\sqrt{m_{swd}}$ , to reflect the data scatter being more than expected from the data uncertainties alone. With further scatter, the switch is made to model 2, at B in Fig. 1. Alternatively, if the user accepts the switch to model 2, then model 1x is not used, indicated by the vertical line at A extending up to the model 2 line in Fig. 1. The model 2 calculation 130 in ISOPLOT is unrelated to YORK. The data uncertainties are discarded and the slope of the line through the linear trend is calculated as the geometric mean of the lines calculated by unweighted least squares of  $y$  on  $x$  and of  $x$  on  $y$  (see Appendix A).

In summary, then, in ISOPLOT the calculation of ages and their uncertainties involves a number of decision points based around the concept of  $m_{swd}$  that impart significant (and in our view unwelcome) step-changes in the way that the data are 135 handled, and algorithms applied. To assist in further discussion of these matters we depart from the language of ISOPLOT at this point, reintroducing the term *errorchron*, counterposed to *isochron*, following Brooks et al. (1972). The idea is that isochrons have a higher chance of having age significance, while *errorchrons* have a lower chance. In particular, it seems to be unhelpful for the results of model 2 calculations to be called *isochrons* as is the case in ISOPLOT, given that there is excess scatter in the data.

## 140 1.2 Replacing ISOPLOT

Given that ISOPLOT's implementation of model 1+2 line fits is the gold standard of *isochron* calculations presently, where are the problems, and then what can be done to address them? A shortcoming in YORK stems from the assumption that data uncertainties are *strictly* Gaussian-distributed. In real-world application this appears to be too restrictive, with datasets that are likely to have age significance being labelled as *errorchrons* because  $m_{swd}$  is too large. While using YORK guided by 145  $m_{swd}$  is optimal statistically if data uncertainties are strictly Gaussian, this logic fails once uncertainties are even slightly non-Gaussian (originally Tukey, 1960). In such circumstances, both  $m_{swd}$  and least squares methods themselves, like YORK, become unreliable (e.g. Hampel et al., 1986; Huber, 1981).

Rather than being truly Gaussian, data uncertainties may well be Gaussian-distributed in their centres, but slightly fat-tailed distant from the centres. An isotopic dataset looks intuitively acceptable if the data has a central linear “spine”, in which scatter 150 is commensurate with stated analytical uncertainty, but this spine is flanked by data of somewhat larger scatter (i.e. excess scatter, from the “fat tail”). This excess scatter may originate in the isotopic analysis or as a result of geological disturbance. Age-significance in such data manifests primarily via the position of the spine. In the following, we focus on this spine in the data.

---

<sup>1</sup>excess scatter occurs when the data distribution has higher variability in the tails than is indicated by the variability of the central part of the distribution, for example if the distribution is Gaussian in the centre but having “fat” tails

Adopting this spine approach, a successful calculation method for a dataset that may not have strictly Gaussian-distributed uncertainties must, firstly, ascertain whether or not such a spine exists in the data—and hence whether calculations yield an isochron or an errorochron. Secondly, in the case of an isochron calculation, the successful method must reliably locate the spine without being perturbed by vagaries in the more scattered data. Classical statistical methods can do neither of these things, tending to be excessively influenced by the data at the extremes of the scatter. However, the field of robust statistics offers calculation methods that can. When a dataset has no excess scatter, reflected in `mswd` lying within an appropriate  $\chi^2$ -constrained confidence interval, such methods can be devised to retrieve identical (or nearly identical) results to classical statistic methods, but, in addition, provide reliable age and age-uncertainty estimates in the presence of excess scatter around a spine. This continuity of operation with increasing `mswd` contrasts with previous approaches and means that the steps in the ISOPLOT line in Fig. 1, which are certainly undesirable, are circumvented. Moreover the involvement of potentially unreliable least squares-based methods, like ISOPLOT model 2, are avoided when the data show excess scatter.

## 2 An Algorithm for Isochron Calculations

An algorithm is sought that finds a robust straight line through a 2-dimensional linear data trend, while converging with the classical statistical approach of YORK for datasets with consistent scatter (i.e. `mswd` passes). This section describes the nature of the problem and the theoretical basis for the robust statistical approach that will be adopted. The algorithm adopted

1. determines a preliminary fit of the data, not dependent on vagaries of the data scatter
2. determines the spine width in relation to this preliminary fit
  - if the spine width is in an acceptable range: isochron
  - if the spine width is not in an acceptable range: errorochron
3. determines a robust fit of the data, starting from the preliminary fit, this fit converging with YORK for “good” data

This algorithm is fleshed out below, and then evaluated via simulated datasets and applied to a natural dataset. The central calculation in the algorithm is detailed in Appendix B, and a `python` implementation is provided in Appendix C.

### 2.1 Uncertainty distributions and data fitting

Geochronological datasets are collected on the presumption that the isotopic compositions were established via an “event” the age of which is to be estimated. Given the focus here on data with linear trends, even if the effect of the event is recorded perfectly by the samples analysed—the isotopic compositions lying on a line—the actual data are measured with finite precision and so the data inevitably scatter about the trend. An uncertainty probability distribution can be used to describe the form of the data scatter.

Classical statistical methods assume that the underlying uncertainty distribution of a dataset is known, typically taken to be Gaussian. Under the Gaussian assumption, if the analytical uncertainty on the measurements have been appropriately inferred,

mswd, the classical statistics parameter used in YORK to validate an isochron, tests that the scatter of datapoints is consistent  
 185 with the inferred uncertainties. But, in general, there is no reason to suppose that a given analytical technique generates a  
 truly Gaussian uncertainty distribution. Even small amounts of geological disturbance destroy the optimality of YORK. If the  
 uncertainty distribution is not strictly Gaussian then classical methods of data fitting become sub-optimal or worse.

While there are many possible non-Gaussian uncertainty distributions, this paper is concerned with a situation commonly  
 occurring in datasets, in which the datapoints form a linear spine with Gaussian-like scatter, but additional scatter is seen in the  
 190 tails of the distribution. Such a dataset still encodes meaningful age information in its spine, yet it will typically fail an mswd  
 test owing to its departure from a Gaussian distribution. In this work, datasets of this nature are modelled using a contaminated  
 Gaussian uncertainty distribution (Gaussian mixture) (e.g. Tukey, 1960). Such distributions are written  $c\%dN$ , meaning that  
 with a probability  $(100 - c)\%$  the distribution involves a standard deviation,  $\sigma$ , but with a probability  $c\%$  the distribution has  
 a standard deviation,  $d\sigma$ , both with a mean of zero (see Powell et al., 2002; Maronna et al., 2019, Sect. 2.1). An example is  
 195  $25\%3N$ , with  $c = 25$  and  $d = 3$ , so that with 25% probability the uncertainty is drawn from  $N(0, 3\sigma)$ , and 75% probability  
 drawn from  $N(0, \sigma)$ , with the  $N(0, s)$  notation indicating a Gaussian distribution with a mean of zero and a standard deviation  
 of  $s$ . Such distributions provide excess scatter suitable for developing and evaluating a robust line-fitting calculation. It does  
 not matter if excess scatter in real data is drawn from a different distribution. Note that with the sample sizes provided by most  
 modern geochronological techniques, it is not necessarily possible to test for Gaussian behaviour, or such departures from  
 200 Gaussian behaviour, although they may be evident on quantile-quantile plots (see below).

## 2.2 Isochrons and errorchrons

In YORK, assuming that the data uncertainties are strictly Gaussian distributed, the probability distribution of mswd provides  
 bounds that can be used to distinguish isochrons from errorchrons (e.g. Wendt and Carl, 1991). These bounds come from a 95%  
 confidence interval on mswd, as discussed in Appendix A. Datasets whose scatter give mswd outside the bounds are deemed  
 205 to be errorchrons, not isochrons. The focus in this paper is on mswd that is too large, indicating excess scatter. Mswd is defined  
 with the residuals,  $r_k$ , the distance in  $y$  of the datapoint,  $k$ , to the line,  $e_k$ , weighted by the uncertainty on this distance,  $\sigma_{e_k}$

$$\text{mswd} = \frac{1}{n-2} \sum_{k=1}^n r_k^2 \quad \text{with} \quad r_k = \frac{e_k}{\sigma_{e_k}} = \frac{a + b x_k - y_k}{b^2 \sigma_{x_k}^2 + \sigma_{y_k}^2 - 2b \sigma_{x_k} \sigma_{y_k} \rho_{x_k y_k}} \quad (1)$$

The line being fitted is  $y = a + b x$ ; datapoint,  $k$ , is  $\{x_k, y_k\}$ ; the analytical uncertainty on  $x_k$ ,  $\sigma_{x_k}$ ; the analytical uncertainty on  
 $y_k$ ,  $\sigma_{y_k}$ ; and the correlation between  $x_k$  and  $y_k$ ,  $\rho_{x_k y_k}$  (see derivation of eq. B4 in Appendix B). Note that the slope,  $b$ , appears  
 210 in the denominator of  $r_k$ , as well as the numerator.

If, instead, data uncertainties are  $c\%dN$ , with unknown  $c$  and  $d$ , or some other contaminated Gaussian distribution then there  
 is no equivalent of the mswd argument to say which datasets should give isochrons rather than errorchrons. The approach  
 advocated here is to use a measure that reflects whether the dataset has a linear spine of “good” data within it. The measure  
 suggested,  $s$ , coined the spine width, is robust, and is defined as

$$215 \quad s = \text{nmad}(r) = 1.4826 \text{ median}(|r_k - \text{median}(r)|) \quad (2)$$

with a normalisation constant<sup>2</sup>, 1.4826. Given that  $s$  is based on a median, its magnitude depends on that half of the data that have the smallest absolute values of centred  $r$ , in other words those that would define a spine. If the data were in fact Gaussian-distributed, it is expected that  $s$  should be in a range about 1 in the same way that  $m_{\text{swd}}$  is, given that  $r$  already involves the analytical uncertainties. The larger is  $s$ , greater than 1, the less pronounced is the linear spine in the data (or the uncertainties have been underestimated). Whereas the 95% confidence interval (95%ci) on  $m_{\text{swd}}$  for Gaussian-distributed uncertainties comes from a well-established probability distribution, with  $(n-2)m_{\text{swd}} \sim \chi_{n-2}^2$  (e.g. Wendt and Carl, 1991), the confidence interval on  $s$  needs to be found by simulation (see Appendix D), with the simulated datasets just involving Gaussian-distributed uncertainties. The intervals are given in this table, Table 1:

$n$	95%ci		$\sqrt{m_{\text{swd}}}$	95%ci		$s$
	low	high	*	low	high	*
5	0.268	1.765	1.614	0.09	1.64	1.48
6	0.348	1.669	1.540	0.17	1.62	1.47
8	0.454	1.552	1.449	0.26	1.58	1.45
10	0.522	1.480	1.392	0.31	1.55	1.43
15	0.621	1.379	1.312	0.40	1.50	1.40
30	0.739	1.260	1.215	0.58	1.39	1.33
60	0.818	1.181	1.151	0.71	1.28	1.23

Whereas 1-sided confidence intervals are advocated in Appendix A—columns marked with an asterisk in the Table—2-sided confidence intervals are also given in the table. Using the asterixed column, for example for a dataset with 10 datapoints ( $n = 10$ ), the dataset is deemed to yield an isochron if the observed  $s$  is less than 1.43. If  $s$  is larger, the dataset gives an errorchron. For isochrons, the age uncertainty is calculated as in Appendix B. For errorchrons, the age uncertainty is not calculated because the data scatter is not consistent with the analytical uncertainties at 95% confidence,  $s$  being larger than the bound.

### 2.3 A robust statistics approach to isochron calculation

We seek a statistical approach to isochron calculation that is *robust* (e.g. Huber, 1981; Hampel et al., 1986), meaning that it is not excessively affected by outliers in the data, while having desirable statistical properties, for example good efficiency (see below). In addition, we require the approach to converge to YORK for a “good” dataset, one with a near-Gaussian uncertainty distribution, allowing seamless compatibility with classical data interpretation. The overall approach adopted will be referred to as SPINE, involving the use of spine width for isochron-errorchron distinction, combined with robust line-fitting. The line-fitting is based on the approach of Huber (1981), as outlined in Maronna et al. (2019), Sect. 2.2.2. Whereas most robust line-fitting methods use the scatter of the data as a scale, data uncertainties having been discarded (e.g. Powell et al., 2002),

<sup>2</sup>the normalisation constant makes  $n\text{mad}(r)$  an unbiased estimator of the standard deviation when the data are Gaussian distributed as the sample size becomes large (e.g. Maronna et al., 2019, Sect. 2.4)



here the data uncertainties are used. This is necessary in order to preserve continuity of the results with YORK, in which the data uncertainties are an integral part of the calculation.

In both the Huber approach in SPINE, and in YORK, a straight line is fitted to a dataset by minimising a function of the residuals,  $r_k$ . In the case of YORK this is just the  $\text{mswd}$ , (1). Since isochron data are generally bivariate with correlated analytical uncertainties in  $x$  and  $y$ , the analytical uncertainty in datapoint  $k$  can be represented as an ellipse as in Fig. 2. The absolute value of the residual for datapoint,  $k$ ,  $r_k$ , is in fact the scaling factor on the size of the ellipse required to expand it or reduce it until it touches the best-fit line (Fig. 2).

The function that is minimised to find the best-fit line can be written  $\sum \rho(r_k)$  for both YORK and SPINE. Whereas in YORK,  $\rho(r_k) = r_k^2$  for all  $r_k$ , in SPINE  $\rho(r_k) = r_k^2$  near the centre of the uncertainty distribution (as in YORK), but downweights datapoints for which the absolute value of the residual is greater than a cut-off value,  $h$ . Thus, in SPINE, and in Fig. 3, the Huber  $\rho$  is

$$\rho(r_k) = \begin{cases} 2hr_k - h^2 & r_k < -h \\ r_k^2 & \text{if } -h < r_k < h \\ 2hr_k - h^2 & r_k > h \end{cases} \quad (3)$$

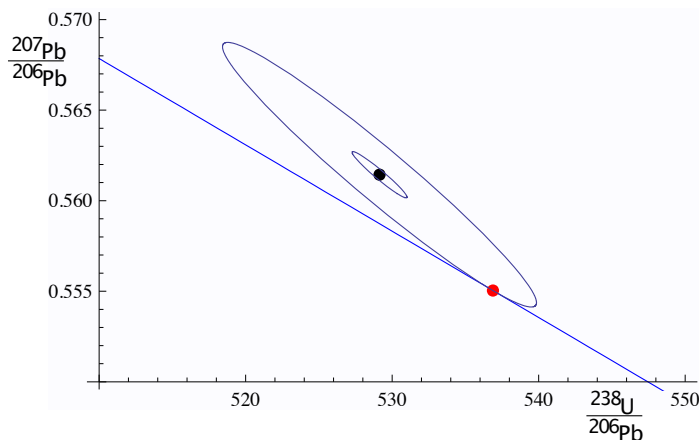


**Figure 2.** For an example datapoint,  $\{x_k, y_k\}$ , the inner ellipse is calculated with the analytical uncertainties,  $V_k$ , at the  $1\sigma$  level (in black). Given a line,  $y = a + bx$  (in blue), the ellipse must be drawn at the  $|r_k|\sigma$  level (in red) to touch the line, in this case  $|r_k| = 5.73$ . The data point is  $x_k = 529.14$ ,  $y_k = 0.5614$ , and  $\sigma_{x_k} = 1.870$ ,  $\sigma_{y_k} = 0.00127$  and  $\rho_{x_k y_k} = -0.967$ . The line is  $y = 0.8108 - 0.0004764x$ .

In SPINE, for residuals that have an absolute value less than an adjustable constant,  $h$ , the contribution to the sum being minimised is the same as for YORK, but it is linear in the residual for larger absolute value. Note that as  $h$  becomes larger and larger, SPINE converges to YORK. The value to use for  $h$  is discussed in Maronna et al. (2019)<sup>3</sup>.

<sup>3</sup>The value used here,  $h = 1.4$ , involves a particular tradeoff between robustness and efficiency (Maronna et al., 2019, Sect. 2.2.2 and 3.4)

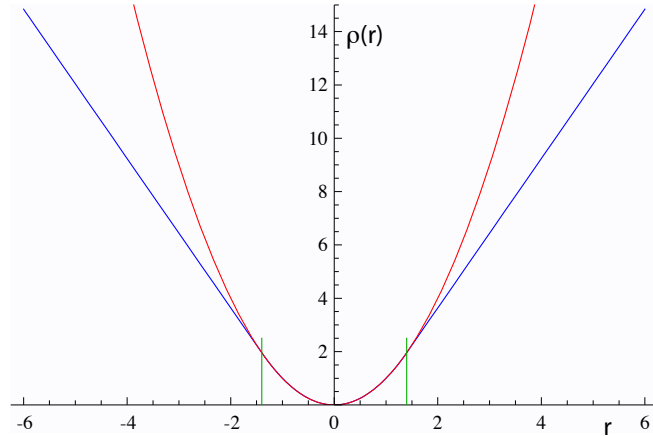


**Figure 3.** Plots of  $\rho(r)$  against  $r$  for YORK in red ( $r^2$ ), and for Huber in SPINE (eq. 3) in blue. The two curves are coincident for  $|r| < h$ , with  $h = 1.4$  the vertical green lines. See text.

The iteration developed in Appendix B minimises  $\sum_k \rho(r_k)$  with respect to the unknown,  $\theta$ , a two-element column vector,  $\{a, b\}^T$  in the line equation,  $y = a + bx$ . The iteration is applicable to SPINE and also YORK. As a starting point of the iteration, data are fit for  $\theta$  with SIEGEL (Siegel, 1982), which is highly robust toward excess scatter. However SIEGEL is much less efficient than SPINE (see below), so SPINE is a better ultimate estimator. A full iteration is envisaged in Appendix B. Once  $\theta$  is calculated, the measure of scatter used to distinguish an isochron from an errorchron can be calculated using Table 1. If an isochron is deemed to have been calculated, the uncertainty on  $\theta$ ,  $\mathbf{V}_\theta$ , can be found, as outlined in Appendix B.

260 The SPINE algorithm can be summarised:

1. determine a preliminary fit of the data using SIEGEL
2. determine the spine width using `nmad`
  - if the spine width is in an acceptable range, from col. 6 in Table 1: isochron
  - if the spine width is not in the acceptable range: errorchron

265 3. determine a robust fit of the data, minimising  $\sum \rho(r_k)$ , with the Huber  $\rho(r_k)$ , (3), starting from the SIEGEL estimate of  $\theta$

## 2.4 Application of SPINE to simulated datasets

Assessing algorithms for data fitting is best done using simulated datasets, so that the true “age” represented by the data is known. In this case, datasets were generated by drawing data points from a range of uncertainty distributions, all centred on a linear trend reflecting an age of 4 Ma. Full details are provided in Appendix D. Two features of the datasets are varied: the number of datapoints in the dataset, and the uncertainty structure adopted, the latter via varying  $c$  and  $d$  in  $c\%dN$ . The

270

algorithm is assessed in terms of its ability to retrieve the specified age of the linear trend on which the simulated datasets are built, and on the uncertainty in the age.

Given that the datasets investigated have fat-tailed contaminated-Gaussian uncertainty distributions, the focus is on the effect of excess scatter in the data, in other words, data scatter over and above what is expected for Gaussian data uncertainties. Nevertheless a small proportion of datasets do have small scatter, giving  $s$  which is below the lower bound for that number of datapoints.

The analysis below compares the results of YORK, applied only to those simulated datasets that lie within the  $m_{swd}$  bounds, with the results of SPINE applied to those datasets that lie within the spine width ( $s$ ) bounds. The greatest majority of the former are included in the latter, e.g.  $> 97\%$  for  $n = 10$ ). Importantly, however, SPINE typically identifies reliable age information in many more datasets than YORK. In the following table,  $m\%excl$  and  $s\%excl$  are the percentage of simulated datasets excluded on the basis of the  $m_{swd}$  and  $s$  bounds, respectively:

$n$	N		5%3N		25%3N		10%10N	
	$m\%excl$	$s\%excl$	$m\%excl$	$s\%excl$	$m\%excl$	$s\%excl$	$m\%excl$	$s\%excl$
5	2.5	2.5	8.7	4.0	30.2	9.8	32.5	9.5
6	2.5	2.5	9.6	3.9	34.6	13.8	37.3	10.9
8	2.5	2.5	12.7	4.2	44.7	14.5	46.0	10.4
10	2.5	2.5	14.2	4.0	51.8	15.2	53.5	9.7
15	2.5	2.5	17.4	4.2	65.2	17.1	68.2	9.1

Note that, for example, for  $n = 10$ , datasets drawn from 5%3N, in fact have  $100(10^{0.95}) = 59.9\%$  of the datasets having all uncertainties Gaussian, while 40.1% have at least one uncertainty drawn from 3 times Gaussian (3N). For 25%3N, 5.6% are Gaussian only, and for 10%10N, 34.9%. The leftmost columns are 2.5% by definition.

A 95% confidence interval on age can be found by ordering the list of ages calculated for the datasets, selecting the the lower limit at the 2.5% point in the list, and the upper limit at the 97.5% point. For datasets that lie within the  $s$  bound in SPINE or  $m_{swd}$  bound in YORK, the 95% confidence intervals on ages are essentially the same, even though a much larger proportion of datasets lie within bounds using SPINE than using YORK. A comparison of ages can also be made between YORK and SPINE for simulated datasets that lie *outside* the  $m_{swd}$  bounds. For  $n = 10$  and Gaussian-distributed data, the 95% confidence interval is  $\pm 0.021$  Ma for both YORK and SPINE, but for 5%3N, 25%3N and 10%10N, the 95% confidence interval on the YORK ages are  $\pm 0.035$ ,  $\pm 0.040$ , and  $\pm 0.092$  Ma, respectively, while the SPINE ages are  $\pm 0.027$ ,  $\pm 0.034$ , and  $\pm 0.034$  Ma. The differences between the ages given by the two methods, normalised by the uncertainties on the SPINE ages, are  $\pm 1.62$ ,  $\pm 1.63$  and  $\pm 5.54$ . Comparison of the intervals shows that the  $m_{swd}$  bounds are relevant to the application of YORK, in that generally it does not work well outside the bounds, while indicating that SPINE is (much) more reliable for age determination for such datasets.

Considering age uncertainty, it might be expected that the uncertainties suffer from the excess scatter in the data in datasets that yield an errorchron with YORK but an isochron with SPINE. This appears not to be the case, but there is a small degradation in the age uncertainties retrieved caused by an unavoidable efficiency loss using SPINE. Efficiency at the Gaussian distribution

is the ratio of the variance obtained by the optimal estimator (YORK), divided by the variance using the chosen robust estimator (in this case, SPINE). SPINE involves an efficiency loss at the Gaussian distribution, which is illustrated in Figure 4 via kernel density estimate (kde) plots of the age uncertainties calculated for simulated datasets with  $n = 10$  and Gaussian-distributed uncertainties. Kde plots are probability distributions akin to smoothed histograms (Wand and Jones, 1995). The red curve is the kde for datasets that have all  $|r_k| < h$ , as would be given by YORK on datasets with Gaussian-distributed uncertainties. The blue curve is the kde for all datasets with at least one  $|r_k| > h$ . The overall kde, in black, is the kde of all of the datasets in the red and blue kde, in observed proportion, about 30% to 70%. The efficiency loss of SPINE is reflected in the displacement of the black curve to slightly higher age uncertainty than the red curve. The relationships shown in Figure 4 for  $n = 10$  can be seen for other  $n$  in Figure 5. The pairs of red and black lines, correspond to, and have the same meaning as the red and black lines in Figure 4. As expected, the distribution of age uncertainties moves towards larger values as the sample size  $n$  decreases.

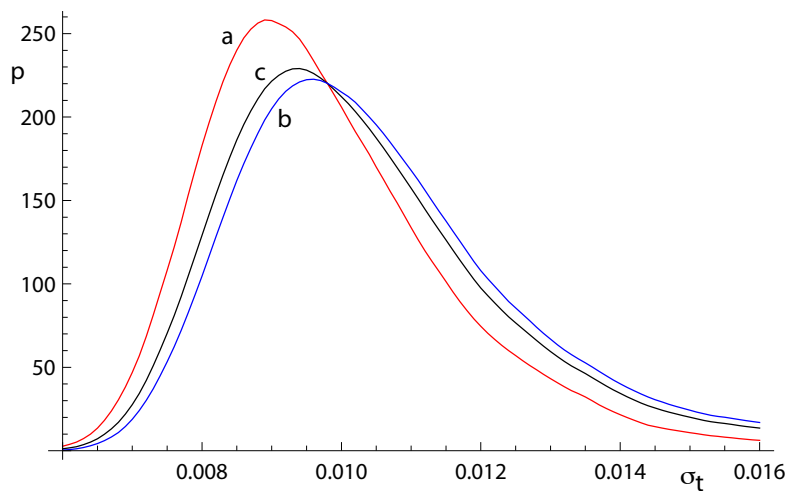


**Figure 4.** Kernel density estimates (kde) for age uncertainty calculated with SPINE on 10,000 simulated datasets with  $n=10$  and Gaussian-distributed uncertainties. (a) Those datasets for which all  $|r_k| < h$  (in red); (b) those datasets for which at least one  $|r_k| > h$  (in blue), and (c) overall result combining a and b in observed proportion (in black).

Whereas SPINE involves an efficiency loss at the Gaussian distribution, it performs better—i.e. it is much more robust—than YORK for data from contaminated Gaussian distributions (e.g. Maronna et al., 2019, Table 2.2). The ability of SPINE to retrieve age uncertainty information for such data varies with the probability and scale of the contamination, as shown in Figure 6. Not unexpectedly the more seriously contaminated distributions (25%3N and 10%10N) involve a greater displacement of the kde to higher age uncertainty than the more weakly contaminated 5%3N distribution. Although the displacement of the blue curves from the black curve is real, nevertheless the ability of SPINE to retrieve age uncertainties from datasets with contaminated distributions is good.

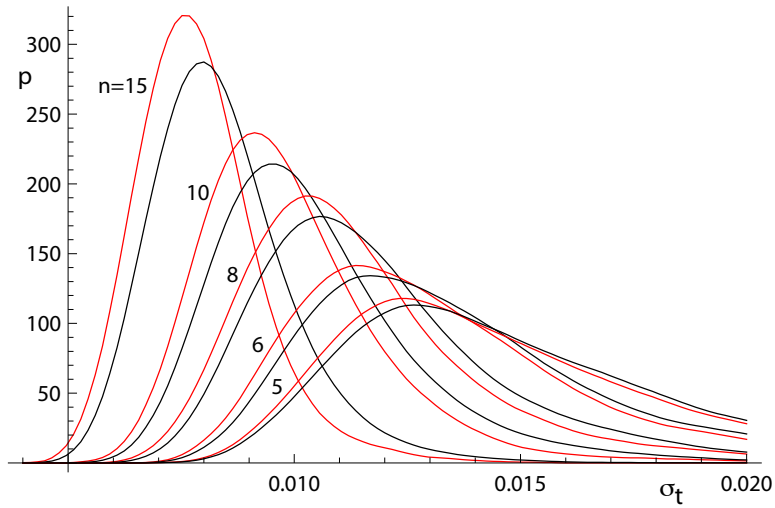


**Figure 5.** Kernel density estimates for age uncertainty calculated with SPINE on 10,000 simulated datasets with a range of  $n$  values and Gaussian-distributed uncertainties. In each case, the  $kde$  for those datasets for which all  $|r_k| < h$  is in red and the overall  $kde$  is in black.

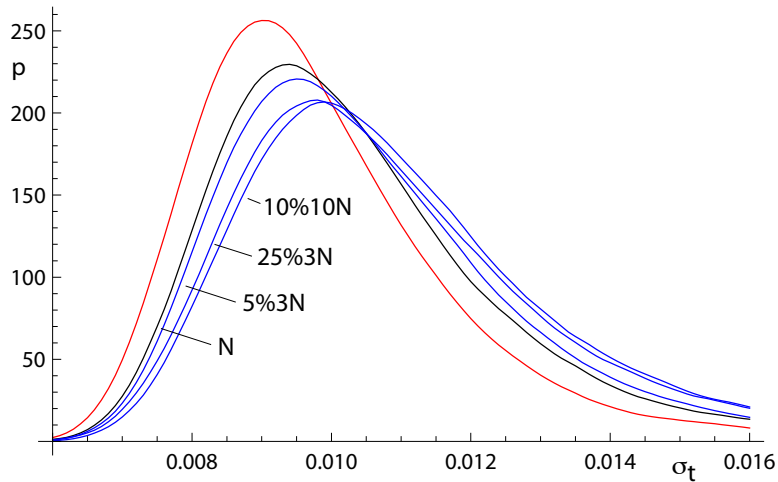


**Figure 6.** Kernel density estimates for age uncertainty calculated with SPINE on 10,000 simulated datasets with  $n=10$  and several uncertainty structures. The  $kde$  for those datasets for which all  $|r_k| < h$  is in red, the  $kde$  for datasets with Gaussian-distributed uncertainties is in black, and the  $kde$  for all of the datasets for 5%3N, 25%3N and 10%10N respectively are in blue.

## 2.5 Application of SPINE to a natural dataset

In order to show the real-world utility of SPINE, we consider data for a carbonate flowstone from the Riversleigh World Heritage fossil site in Queensland, Australia (Sample 0708). Isotope dilution U-Pb data for the bulk sample were previously

published by Woodhead et al. (2016) providing a Model 2 isochron with an age of  $13.72 \pm 0.12$  Ma and with a  $m_{swd}$  of 3.7.

320 The new data presented here were obtained by laser ablation ICPMS on the same sample using methods outlined and published in Woodhead and Petrus (2019). Such datasets are typically larger with little error correlation (rounder error ellipses), but with larger uncertainties than isotope dilution data. These new data define an errorchron under the YORK assumptions, with  $m_{swd} = 1.68$ , and a model 2 age of  $13.68 \pm 0.31$  Ma. These data might therefore be rejected under the  $m_{swd}$  criterion despite exhibiting a well-developed linear trend. With SPINE,  $s = 1.24$ , within the  $s$  range for an isochron, the age is  $13.69 \pm 0.26$  Ma ( $\pm$  is

325  $1.96\sigma$ ). The data for 0708 are plotted in Fig. 7, with 95% confidence ellipses on the datapoints. Further calculations with this sample, comparing the results of our new algorithm with existing approaches are presented in Appendix A.

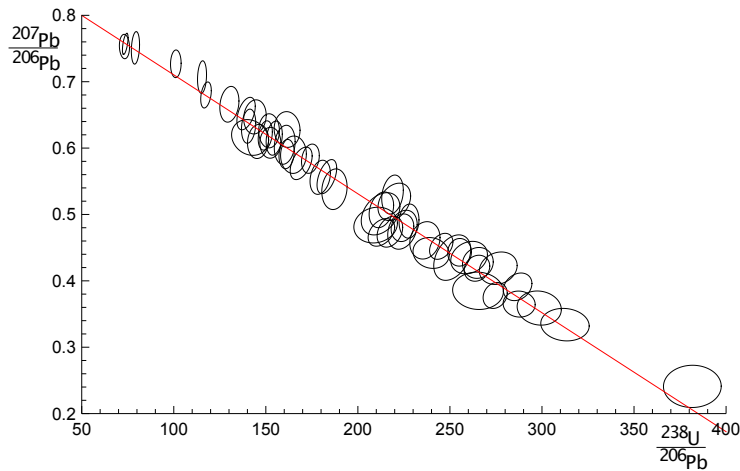


**Figure 7.** Laser ablation example 0708. See text.

With 0708, the SPINE and ISOPLOT ages are very similar, but  $m_{swd}$  suggests an errorchron, so there is excess scatter on this basis. Quantile-quantile plots can be used to show the nature of the distribution of the residuals that contribute to such excess scatter. Here, Fig. 8, the ordered residuals normalised to  $n_{mad}(r)$  are plotted against the quantiles of the standard Gaussian distribution,  $N(0, 1)$  (see Fox, 2016, Sect 3.1.3). The normalisation means that if the residuals are Gaussian-distributed, they should plot close to a line of unit slope through the origin. The figure also includes 95% pointwise confidence intervals (blue dashed lines). The figure suggests that the residuals are in fact effectively Gaussian-distributed, lying between the blue-dashed lines (and  $m_{swd}$  has been too sensitive in flagging that the residuals are not Gaussian-distributed).

330

Generally, geochronological datasets do not have obvious outliers—they might be “cleaned” of isolated datapoints before an age calculation, or the dataset might even be discarded. But many of the simulated datasets from contaminated Gaussian distributions, as used above, do contain outliers. In Appendix E an example of a simulated dataset with outliers (from 25%3N) is used to show how YORK and SPINE behave, and to show what a quantile-quantile plot looks like in those circumstances.

335

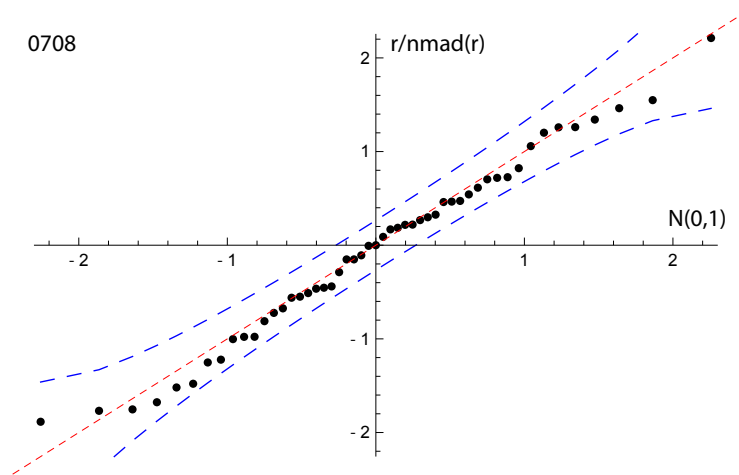


**Figure 8.** Quantile-quantile plot for sample 0708, using the SIEGEL fit of the data to calculate the residuals to plot. The dashed red line has unit slope through the origin; the blue dashed lines are the 95% pointwise confidence intervals. See text.

### 3 Discussion

This work was motivated by the belief that many isotopic datasets contain meaningful age information that cannot be identified using classical statistical methods and may therefore be discarded or discounted. In such cases, the age information is contained in a linear spine in the data, but the data also contains scatter that is inconsistent with a Gaussian uncertainty distribution, having fatter tails than Gaussian. A statistical test based on the spine width is devised, akin to using  $m_{swd}$  in classical methods, allowing an isochron-errorchron distinction to be made. Many datasets that give isochrons based on the spine width, give errorchrons under the assumption of a strict Gaussian uncertainty distribution. A statistically-robust isochron calculation method is able to retrieve this age information and to provide appropriate uncertainty estimates. Calculated ages and age uncertainties are more reliable than ISOPLOT ones for data with excess scatter.

Contaminated Gaussian distributions provide a model for a type of dataset with excess scatter relative to a strictly Gaussian-distributed one. The robust isochron method presented in this work can however be applied *in general* to data which is Gaussian-distributed only in the central spine of the uncertainty distribution, with non-Gaussian scatter occurring in the tails, arising from analytical or geological uncertainty. Indeed, it can be applied to any dataset with a well-developed spine in the data.

In most robust statistics data fitting approaches, the formal uncertainties output during data measurement are ignored. Instead, the scale used in the data fitting is derived from the scatter in the data themselves, an approach adopted by Powell et al. (2002). The new approach followed here *does* include the data measurement uncertainties, and this allows the results to converge on those of YORK when the data *lack* excess scatter. This provides compatibility with older “good” datasets processed using the classical statistical approach but, going forward, allows age information to be extracted from a much wider range of datasets which might otherwise be rejected for having  $m_{swd}$  greater than the isochron cutoff.

A problem with SPINE, shared with YORK, is that the effect of high-leverage data is not taken into account. Such data are easily recognised in  $x$ - $y$  plots, when a small proportion of the data—even one datapoint—is separated from the main body of the data along the trend through the data. Data fitting tends to be overly constrained to fit high-leverage data, giving them small residuals, even if the best fit of the main body of the data alone would give the high-leverage data larger residuals. In 0708, the point at highest  $x$  is relatively high leverage ( $\hat{h} = 0.171$ ). Robust approaches have been developed to handle high leverage data, e.g. Maronna et al. (2019), ch. 5, but are not yet developed for the situation where the data uncertainties are taken into account, nor for the relatively small datasets that are typical of geochronological studies (c.f. Fig. 7). Huber and Rochetti (2009), ch. 7, have a counter view advocating data assessment, rather than aiming for a black-box method to try and automatically safeguard against the potentially deleterious effect of high leverage data, an approach we suggest here. In the case of the relatively high leverage datapoint in 0708, omitting this datapoint gives  $13.75 \pm 0.27$  Ma (compare row 11 with row 1 in the Table in Appendix A), within uncertainty of the age including this datapoint.



## Appendix A: Algorithms and applications to sample 0708

Here are collected some results of calculations for sample 0708, used in Fig. 7, and some related algorithmic details.

### 370 thought experiment in Fig. 1

The thought experiment sketched in Fig. 1 aimed to show the consequence for ISOPLOT behaviour of the modification of the observed data in a dataset to reduce or increase the scatter about the linear trend. The calculated equivalent of Fig. 1 for sample 0708 is shown in Fig. A1, including also the corresponding SPINE results. In calculating the Figure, the modification of the dataset is achieved by first taking the data points with their attendant error ellipses (i.e. covariance matrices), and moving them  
375 all in to lie on the linear trend, considered as fixed by a YORK calculation. Then the points and ellipses are considered to be displaced away from the trend. This is “move” in the Table below, going from -1, when the points lie on the trend, through 0, with the points as in the original data, to positive when displaced further away from the trend. “Move” varies more or less linearly with  $\sqrt{m_{swd}}$  from -0.133 at the left-edge of the Figure, to 0.064 on the right-edge; the spine width changes from 1.08 to 1.32 across the Figure. For these calculations the last line in the dataset is omitted as it is relatively high leverage ( $\hat{h} =$   
380 0.171), not wishing this datapoint to affect the results.

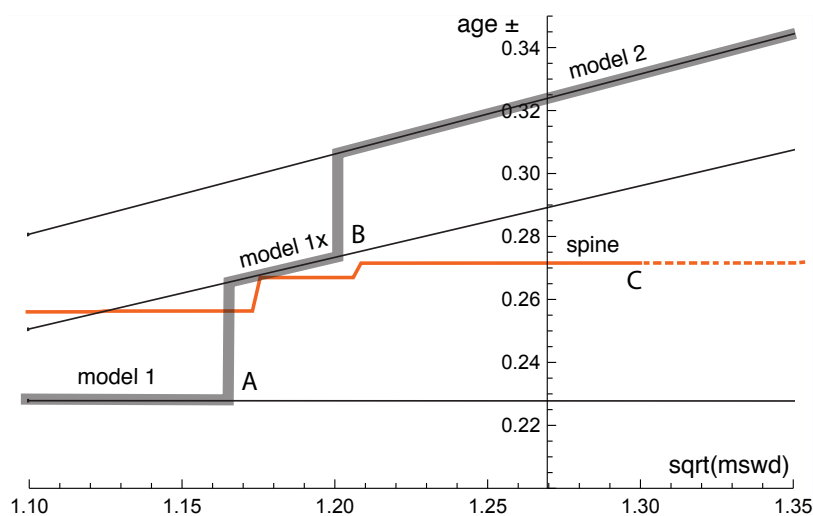


**Figure A1.** Age uncertainty ( $age \pm$ ) plotted against  $\sqrt{m_{swd}}$  under the ISOPLOT protocol for the progressively modified dataset, 0708 (see text). In model 1, the age uncertainty is constant with increasing data scatter (reflected in increasing  $m_{swd}$ ), until there is a step change in age uncertainty at A when the  $\pm$  is multiplied by  $\sqrt{m_{swd}}$ . Then at B there is another step change with further increase of data scatter to model 2 (see text). The location of the step at A is based on a 95% confidence interval for  $m_{swd}$  (discussed below), whereas the  $\sqrt{m_{swd}}$  position of the step at B is arbitrary. The  $y$ -axis is drawn at the  $\sqrt{m_{swd}}$  of the actual data, 1.27 (i.e. no modification of the data). See text.

In the Figure, extending from the left, through  $m_{swd} = 1$ , to A, the ISOPLOT age uncertainty (model 1, i.e. YORK) is constant because the data scatter is consistent with the data uncertainties. Through this range the SPINE age uncertainty is above the

model 1 line because of the efficiency loss embodied in SPINE, as shown in Figs 4–5. However, after the age uncertainty steps with increasing  $m_{swd}$ , to the right of the diagram, the SPINE age uncertainty is smaller than the model 1x and model 2 age uncertainty. This is because SPINE gives an isochron on the basis of spine width up to C at  $\sqrt{m_{swd}} \approx 1.3$ , whereas model 2 is an errorchron, on the basis of the assumption of strictly Gaussian data uncertainties. The small steps in the SPINE age uncertainty line are an artefact of the approximation used in the calculation of the age uncertainty, see Appendix B.

In the top part of the following Table, the results for SPINE and for ISOPLOT are summarised. The  $\Delta$  column gives the change to the age from the SPINE age, normalised by the uncertainty on the SPINE age. Below the double line in the Table, are some results from the above thought experiment, Fig. A1.

		move	$\sqrt{m_{swd}}$	age	age $\pm$	$\Delta$	notes
1	SPINE			13.685	0.257	–	$s = 1.24$
2	YORK		1.296	13.733	0.216	0.37	outside 95% c.l.
3	ISOPLOT model 1x			13.733	0.280		
4	ISOPLOT model 2			13.679	0.306	–0.05	
5	siegel			13.803		–0.95	
6	SPINE	–0.133	1.1	13.769	0.252		$s = 1.08$
7	YORK			13.800	0.223	–0.39	inside 95% c.l.
8	SPINE	–0.055	1.2	13.756	0.262		$s = 1.18$
9	ISOPLOT model 1x			13.800	0.268	–0.39	
10	ISOPLOT model 2			13.832	0.300	–0.62	
11	SPINE	0	1.27	13.747	0.267	–	$s = 1.25$ $\Delta = 0.366$
12	ISOPLOT model 2			13.836	0.317	–0.65	
13	SPINE	0.024	1.3	13.743	0.267		$s = 1.26$
14	ISOPLOT model 2			13.837	0.325	–0.66	

Additional algorithmic details for ISOPLOT follow next, in part related to the above thought experiment.

### ISOPLOT model 1

In the ISOPLOT *model 1* calculation, i.e. in YORK, a decision has to be made about the confidence interval on  $m_{swd}$  that is used to denote the range of data scatter (i.e.  $m_{swd}$ ) that is considered to be accounted for by the data uncertainties, without need to either multiply the age uncertainty by  $\sqrt{m_{swd}}$  (i.e. model 1x), or switch directly to an alternative calculation (which is model 2 in ISOPLOT). On the understanding that data uncertainties are correctly assigned, a one-sided confidence interval on  $m_{swd}$  can be adopted, acknowledging that  $m_{swd}$  is not being used to identify the case where assigned data uncertainties are too large or too small. The upper end of the confidence interval on  $m_{swd}$  is where excess scatter is considered to start, a conventional choice being derived from a 95% confidence interval. Note that there is no argument that this should be at  $m_{swd} = 1$  (c.f.

Dickin, 2005, p37), unless the number of datapoints is huge. Even for a dataset of 50 datapoints the 95% confidence interval on  $m_{swd}$  extends to 1.36. In terms of the *probability of fit* measure used in ISOPLOT, this is  $100 - 95 = 5\%$ . It might be noted that the naming of probability of fit seems unhelpful - it is clearer to focus on  $m_{swd}$ .

## ISOPLOT model 2

405 The so-called *error-in-variables* ( $e_{iv}$ ) or measurement-error problem is avoided in YORK because the uncertainty in the  $x$  variable is taken into account explicitly. If it was not, then  $e_{iv}$  results in the calculated slope being biased downwards and the approach being inconsistent (e.g. Fuller, 1987).

In the ISOPLOT *model 2* calculation,  $e_{iv}$  is avoided, even though the data uncertainties are discarded, by making the slope of the line through the data be the geometric mean of the slopes of ordinary least squares of  $y$  on  $x$ ,  $b_{yx}$ , and  $x$  on  $y$ ,  $1/b_{xy}$ .

410 These are

$$b_{yx} = \frac{\sum(x_k - \bar{x})(y_k - \bar{y})}{\sum(x_k - \bar{x})^2} \quad \text{and} \quad \frac{1}{b_{xy}} = \frac{\sum(x_k - \bar{x})(y_k - \bar{y})}{\sum(y_k - \bar{y})^2}$$

with  $\bar{x} = \frac{1}{n} \sum x_k$  and  $\bar{y} = \frac{1}{n} \sum y_k$ . Then

$$b = \pm \sqrt{b_{yx} b_{xy}} = \pm \sqrt{\frac{\sum(y_k - \bar{y})^2}{\sum(x_k - \bar{x})^2}} \quad \text{and} \quad a = \bar{y} - b\bar{x}$$

with, in this case, the sign of the square root being negative. The calculation in ISOPLOT does not use this explicit formula, 415 instead adopting an algebraic equivalent that allows the YORK iteration to be used.

## ISOPLOT robust

In ISOPLOT, there is an option to use a *robust* isochron calculation method. The two available have high breakdown point but low efficiency (e.g. Huber, 1981, Sect. 1.2.3). The second method—(Siegel, 1982)—can be considered to supercede the first. In fact, here, SIEGEL is used in the implementation of SPINE as a starting point for the iteration (see Appendix C). The fit of 420 the data for sample 0708 with SIEGEL is given in line 5 of the Table.

## Appendix B: Iteration in SPINE

The SPINE algorithm involves minimising  $\sum_k \rho(r_k)$  with respect to the unknown,  $\theta$ , a two-element column vector,  $\{a, b\}^T$  in the line equation,  $y = a + bx$ , in order to fit the data. The residual,  $r_k$  on datapoint  $k$  is defined below, and the function  $\rho$  is defined in (3) in the main text. [The SPINE algorithm subsumes YORK.](#)

425 Writing the  $k$ th datapoint as  $\{x_k, y_k\}$ , generally the isotopic data used in isochron calculations involve uncertainties in both  $x_k$  and  $y_k$ , and commonly the  $x_k$  and  $y_k$  are also correlated. These can be represented by a covariance matrix,  $V_k$ ,

$$V_k = \begin{bmatrix} \sigma_{x_k}^2 & \sigma_{x_k} \sigma_{y_k} \rho_{x_k y_k} \\ \sigma_{x_k} \sigma_{y_k} \rho_{x_k y_k} & \sigma_{y_k}^2 \end{bmatrix} \quad (\text{B1})$$

in which  $\sigma_{x_k}$  is the standard deviation on  $x_k$ ,  $\sigma_{y_k}$  the standard deviation on  $y_k$ ,  $\sigma_{x_k}\sigma_{y_k}\rho_{x_k y_k}$  the covariance between  $x_k$  and  $y_k$ , and  $\rho_{x_k y_k}$  the correlation coefficient between  $x_k$  and  $y_k$ . The covariance matrix can be represented by an ellipse around the  
 430 data point in an  $x$ - $y$  diagram, as illustrated in Fig. 2. The residual,  $r_k$ , a measure of the distance of the point  $\{x_k, y_k\}$  to the line, is calculated from the coordinates of the data points,  $\{x_k, y_k\}$ , and their uncertainties in  $V_k$ , by

$$r_k = \frac{e_k}{\sigma_{e_k}} \quad (\text{B2})$$

in which  $e_k$  is the distance of the datapoint from the line,  $e_k = a + bx_k - y_k$ , and  $\sigma_{e_k}$  is the standard deviation on  $e_k$ . The standard deviation,  $\sigma_{e_k}$ , is calculated by error propagation using  $V_k$ :

$$435 \sigma_{e_k}^2 = \left\{ \frac{\partial e_k}{\partial x_k}, \frac{\partial e_k}{\partial y_k} \right\} V_k \left\{ \frac{\partial e_k}{\partial x_k}, \frac{\partial e_k}{\partial y_k} \right\}^T = b^2 \sigma_{x_k}^2 + \sigma_{y_k}^2 - 2b \sigma_{x_k} \sigma_{y_k} \rho_{x_k y_k} \quad (\text{B3})$$

with the term in curly brackets evaluating to  $\{b, -1\}$ . The residual is then

$$r_k = \frac{e_k}{\sigma_{e_k}} = \frac{a + bx_k - y_k}{\sqrt{b^2 \sigma_{x_k}^2 + \sigma_{y_k}^2 - 2b \sigma_{x_k} \sigma_{y_k} \rho_{x_k y_k}}} \quad (\text{B4})$$

In matrix form, the residuals can be written as a column vector,  $\mathbf{r}$

$$\mathbf{r} = \mathbf{W}_e \mathbf{e} = \mathbf{W}_e (\mathbf{X}\boldsymbol{\theta} - \mathbf{y}) \quad (\text{B5})$$

440 with  $\mathbf{W}_e$  a diagonal matrix with  $kk$ th element,  $1/\sigma_{e_k}$ .

The minimisation of  $\sum_k \rho(r_k)$  is iterative, starting from a robust but low efficiency estimate of the line, for example using Siegel (1982). The minimisation of  $\sum \rho(r_k)$  is undertaken using the fact that, at the minimum, the derivative of  $\sum \rho(r_k)$  with respect to  $\boldsymbol{\theta}$  is zero. Defining

$$2\psi(r_k) = \frac{\partial \rho(r_k)}{\partial r_k} \quad (\text{B6})$$

445 this function, for the Huber (1981) approach, from (3), is

$$\psi(r_k) = \begin{cases} -h & r_k < -h \\ r_k & \text{if } -h < r_k < h \\ h & r_k > h \end{cases} \quad (\text{B7})$$

For YORK,  $\psi(r_k) = r_k$ , equivalent to SPINE with large  $h$ .

At the minimum of  $\sum \rho(r_k)$

$$\sum_k \frac{\partial \rho(r_k)}{\partial \boldsymbol{\theta}} = 0 = \sum_k \left( \frac{\partial \rho(r_k)}{\partial r_k} \right) \left( \frac{\partial r_k}{\partial \boldsymbol{\theta}} \right) = \sum_k \psi(r_k) \left( \frac{\partial r_k}{\partial \boldsymbol{\theta}} \right) = \sum_k \psi(r_k) \frac{1}{\sigma_{e_k}} \left\{ \left( \frac{\partial e_k}{\partial \boldsymbol{\theta}} \right) - r_k \left( \frac{\partial \sigma_{e_k}}{\partial \boldsymbol{\theta}} \right) \right\} \quad (\text{B8})$$

450 In the curly braces, writing the first derivative,  $\{1, x_k\}$ , as the  $k$ th row of a matrix  $\mathbf{X}$ , and writing the first and second derivatives together as the  $k$ th row of a matrix  $\mathbf{X}'$ , then the  $k$ th row of  $\mathbf{X}'$  is

$$X'_k = \{1, x'_k\} = \left\{ 1, x_k - \frac{r_k}{\sigma_{e_k}} (b \sigma_{x_k}^2 - \sigma_{x_k} \sigma_{y_k} \rho_{x_k y_k}) \right\}$$

with  $b$  the slope of the line. The second column of  $\mathbf{X}$  is simply the data  $x$  values, while the second column of  $\mathbf{X}'$  is the  $x$  values on the line where the uncertainty ellipses around each datapoint would touch it,  $\mathbf{x}'$ . In matrix form, (B8) can be written as

$$455 \quad \mathbf{X}'^T \mathbf{W}_e \psi(\mathbf{r}) = 0 \quad (\text{B9})$$

in which  $\psi(\mathbf{r})$  is a column vector whose  $k$ th element is  $\psi(r_k)$ . B9 constitutes two non-linear equations requiring iteration to solve. Two iteration schemes are proposed. The first iteration, in fact used for all the simulations, proceeds directly from (B9), while the second iteration is in iteratively reweighted least squares form (e.g. Maronna et al., 2019, Sect. 4.5.2).

In the first scheme, at iteration  $i$ , progressing towards the minimum with  $\theta_i = \theta_{i-1} + \Delta\theta$ , for  $|r_k| < h$ ,  $\psi_i(r_k) = \psi_{i-1}(r_k) +$   
 460  $X_k \Delta\theta / \sigma_{e_k}$  and  $\psi_i(r_k) = \psi_{i-1}(r_k)$  otherwise. This can be written  $\psi_i(r_k) = \psi_{i-1}(r_k) + \dot{\psi}_{i-1}(r_k) X_k \Delta\theta / \sigma_{e_k}$ , in which  $\dot{\psi}(r_k) = \partial\psi(r_k) / \partial r_k$ , which is 1 for  $|r_k| < h$ , and 0 otherwise, from (B7). Substituting into (B9) gives

$$\mathbf{X}'^T \mathbf{W}_e (\mathbf{W}_e \mathbf{I}' \mathbf{B} \Delta\theta + \psi(\mathbf{r})) = 0 \quad (\text{B10})$$

dropping iteration subscripts, with  $\mathbf{I}' = \text{diag}(\dot{\psi}(\mathbf{r}))$  a modified identity matrix with its  $kk$ th element equal to  $\dot{\psi}(r_k)$ . Equation (B10) can then be rearranged to give  $\Delta\theta$  at the current iteration

$$465 \quad \Delta\theta = -(\mathbf{X}'^T \mathbf{W}_e^2 \mathbf{I}' \mathbf{X})^{-1} \mathbf{X}'^T \mathbf{W}_e \psi(\mathbf{r}) \quad (\text{B11})$$

Iteration proceeds until  $\Delta\theta$  approaches 0.

The second iteration scheme is the iteration implemented in the python code. Such iterations are known to be stable, e.g. Maronna et al. (2019). However the logic of the first scheme is needed to obtain the covariance matrix of  $\theta$ , below. In the second scheme, a weight function,  $w(r_k)$ , is introduced so that the resulting equations have a simple least squares form. For  
 470 (B9), this can be done by defining  $w(r_k) = \psi(r_k) / r_k$ , so that  $\psi(r_k) = r_k w(r_k)$ , introducing  $\mathbf{r}$  explicitly into (B9). Then

$$\mathbf{X}'^T \mathbf{W} (\mathbf{X}\theta - y) = 0 \quad (\text{B12})$$

in which the  $kk$ th element of the diagonal matrix,  $\mathbf{W}$ , is  $w(r_k) / \sigma_{e_k}^2$ , combining the weighting from  $w$  with the weighting from the data uncertainties,  $\mathbf{W}_e$ . By rearranging (B12), the repeated substitution solution to (B9) is given by

$$\theta = (\mathbf{X}'^T \mathbf{W} \mathbf{X})^{-1} \mathbf{X}'^T \mathbf{W} y \quad (\text{B13})$$

475 Iteration is needed as  $\mathbf{X}'$  and  $\mathbf{W}$  depend slightly on  $\theta$ , given a sensible starting point for the iteration as provided by SIEGEL.

Accepting that an isochron has been calculated, the covariance matrix of  $\theta$ ,  $\mathbf{V}_\theta$ , can be calculated by error propagation of the data to  $\theta$  using the logic of the first iteration scheme. First it is convenient to transform the problem solved by (B11) to an identical one in which the data are represented by  $\mathbf{e}$  rather than  $\{\mathbf{x}, \mathbf{y}\}$ . First note that (B9) involves  $\mathbf{r}$ , a scalar for each data point, the uncertainty on  $\mathbf{e}$  in  $\mathbf{W}_e$ , and the  $x$  position on the best-fit line where the ellipse around each datapoint touches the  
 480 line, at  $\mathbf{x}'$ , the second column of  $\mathbf{X}'$ . Given the best-fit  $\theta$ , the  $y$  corresponding to  $\mathbf{x}'$ , is  $y' = \mathbf{X}'\theta$ . Defining  $\mathbf{y}'' = \mathbf{y}' - \mathbf{e}$ , data involving  $\{\mathbf{x}', \mathbf{y}''\}$ , rather than  $\{\mathbf{x}, \mathbf{y}\}$ , is an identical problem via (B9). In this identical problem,  $\mathbf{x}'$  and  $\mathbf{y}'$  are fixed (have no uncertainty). With this, the change in  $\theta$  corresponding to (B9), becomes

$$\Delta\theta = -(\mathbf{X}'^T \mathbf{W}_e^2 \mathbf{I}' \mathbf{X}')^{-1} \mathbf{X}'^T \mathbf{W}_e \psi(\mathbf{r}) \quad (\text{B14})$$

in terms only of  $\mathbf{X}'$  and not involving  $\mathbf{X}$ . This is akin to the transform in York et al. (2004) to convert the  $\mathbf{V}_\theta$  of York (1969) to that of the  $\mathbf{V}_\theta$  of Titterton and Halliday (1979).

Assuming that  $\theta$  is approximately linear in each  $e_k$  around the minimum in  $\sum \rho(r_k)$ , then

$$\mathbf{V}_\theta = \left( \frac{\partial \theta}{\partial \mathbf{e}} \right) \mathbf{V}_e \left( \frac{\partial \theta}{\partial \mathbf{e}} \right)^T \quad (\text{B15})$$

At the solution of (B9),  $\Delta\theta = 0$ , so, by the chain rule using (B14)

$$\left( \frac{\partial \theta}{\partial \mathbf{e}} \right) = \left( \frac{\partial \Delta\theta}{\partial \theta} \right)^{-1} \left( \frac{\partial \Delta\theta}{\partial \mathbf{e}} \right) = (\mathbf{X}'^T \mathbf{W}_e^2 \mathbf{I}' \mathbf{X}')^{-1} \mathbf{X}'^T \mathbf{W}_e^2 \mathbf{I}' \quad (\text{B16})$$

490 Substituting into (B15), cancelling and using  $\mathbf{W}_e^2 \mathbf{I}' \mathbf{W}_e^{-2} \mathbf{I}' \mathbf{W}_e^2 = \mathbf{W}_e^2 \mathbf{I}'$

$$\mathbf{V}_\theta = (\mathbf{X}'^T \mathbf{W}_e^2 \mathbf{I}' \mathbf{X}')^{-1} \quad (\text{B17})$$

The small steps in the age uncertainty (age $\pm$ ) curve in Fig A1 arise when diagonal elements in  $\mathbf{I}'$  change from one to zero as mswd increases.

In YORK (or if all  $|r_k| < h$  in SPINE), then  $\mathbf{I}' = \mathbf{I}$  and  $\psi(\mathbf{r}) = \mathbf{r}$ . So

$$495 \quad \Delta\theta = -(\mathbf{X}'^T \mathbf{W}_e^2 \mathbf{X}')^{-1} \mathbf{X}'^T \mathbf{W}_e \mathbf{r} \quad (\text{B18})$$

and the covariance matrix becomes

$$\mathbf{V}_\theta = (\mathbf{X}'^T \mathbf{W}_e^2 \mathbf{X}')^{-1} \quad (\text{B19})$$

If, in addition, all  $\sigma_{x_k} = 0$  then  $\mathbf{X}' = \mathbf{X}$ , and iteration is not involved,  $\mathbf{e}$  is replaced by  $-\mathbf{y}$ , and

$$\theta = (\mathbf{X}^T \mathbf{W}_e^2 \mathbf{X})^{-1} \mathbf{X}^T \mathbf{W}_e^2 \mathbf{e} \quad (\text{B20})$$

500 with a covariance matrix of

$$\mathbf{V}_\theta = (\mathbf{X}^T \mathbf{W}_e^2 \mathbf{X})^{-1} \quad (\text{B21})$$

These are the results for fitting data by simple weighted least squares.

### Appendix C: SPINE Python code

The second iteration in Appendix B is coded in the Python function, `huber2`. The starting point for the iteration is provided by the function, `siegel` (Siegel, 1982). The calling function, `recipe`, is a placeholder for a more general function to be written by the user.

```
import sys
import datetime
```

```

import numpy as np
510
out = open("out.txt", "w") # opening output file
screen = sys.stdout
standard = [screen, out] # default where print goes

515 default_h = 1.4 # default h in huber

def siegel(data): # siegel (1982)
    n = data.shape[0];
    (x, sdx, y, sdy, cor) = np.transpose(data)
520 x += 1e-8 * np.random.random(n) # naive breaking of x ties
    med = np.empty(n);
    for i in range(n):
        col = np.empty(n);
        for j in range(n):
525             if i is not j: col[j] = (y[j] - y[i])/(x[j] - x[i])
        med[i] = np.median(np.delete(col, i))
    b = np.median(med)
    return np.array((np.median(y - x * b), b))

530 # -----

def calcage(theta, covtheta = None, method = 1):
# tera-wasserburg: focus on lower intercept
    dc238 = 1.55125e-10; dc235 = 9.8485e-10
535 tc = 0; t = t1 = 1500.; tdiff = 1e-4
    (a, b) = theta
    k = 0
    while k < 12 and abs(t - tc) > tdiff:
        tc = t; t = 1/dc238 * np.log(1 + 1/t1)
540 t1 = (1/137.8 * (np.exp(dc235 * t) - 1) / (np.exp(dc238 * t) - 1) - a) / b
        k += 1
    if covtheta is None:
        sdage = 0
    else:
545 den = b * np.exp(dc238 * t) * dc238 + \
        (-np.exp(dc235 * t) * dc235 + np.exp(dc235 * t + dc238 * t) * dc235 + \
        np.exp(dc238 * t) * dc238 - np.exp(dc235 * t + dc238 * t) * dc238)/137.8
        jac = [(np.exp(dc238 * t) - 1)/den * (np.exp(dc238 * t) - 1), (np.exp(dc238 * t) - 1)/den]
        sdage = np.sqrt(np.dot(np.dot(jac, covtheta), np.transpose(jac)))/1e6
550 return (t/1e6, sdage)

# -----

```

```

def huber2(data0, h = 1.4):
555 #   iteratively-reweighted huber line-fitter
    n = data0.shape[0]
    itmax = 20; mindel = 1e-8; mincond = 1e-12; minsump = 0.01
    (x, sdx, y, sdy, cor) = np.transpose(data0)
    avx = np.dot(x, np.ones(n))/n;  avy = np.dot(y, np.ones(n))/n;
560 div = np.array([1/avy, avx/avy])
    data = np.copy(data0)
    (x, sdx, y, sdy, cor) = np.transpose(data)
    x /= avx; sdx /= avx; y /= avy; sdy /= avy; cov = sdx*sdy*cor
    theta = siegel(data);
565 k = 0; code = 0; deltheta = (1e10, 1e10)
    while k < itmax and ( np.sqrt(np.dot(deltheta,deltheta)) > mindel):
        k += 1; (a, b) = oldtheta = theta
        e = a + b * x - y;  sde = np.sqrt(b**2*sdx**2 - 2*b*cov + sdy**2)
        r = e/sde
570 wh = [1 if abs(rk) < h else np.sqrt(h/abs(rk)) for rk in r]/sde
        xp = x - r * (b*sdx**2 - cov)/sde          # x on the line
        ypp = (y - e - r*(b*cov - sdy**2)/sde)*wh  # W^(1/2) (y'-e): y off the line
        c = np.transpose([wh, xp*wh])             # W^(1/2) X'
        (u, s, v) = np.linalg.svd(c, full_matrices=False)
575 if mincond * s[0] > s[1]: code = -1; break  # (nearly) singular matrix
        theta = np.dot(np.dot(np.dot(np.transpose(v), np.diag(1/s)), np.transpose(u)), ypp)
        deltheta = theta - oldtheta
    if k == itmax: code = 1 # not converged
    pc = np.dot([wh**2, xp*wh**2], e);
580 sump = np.sqrt(np.dot(pc, pc));
    if sump > minsump: code = 2 # not solved the nle
    dpsi = [1 if abs(rk) < h else 0 for rk in r]
    covtheta = np.linalg.inv(np.dot(np.dot(np.transpose(c), np.diag(dpsi)), c)) / \
        np.array([[div[0]**2, div[0] * div[1]], [div[0] * div[1], div[1]**2]])
585 return (code, theta/div, covtheta, sump, k, s[1])

# -----

def pr(s, e="\n", printto=standard):
590 # prints a string
    for pr in printto: print(s, end=e, file=pr)

def recipe(title, data, where = [screen]):
# prototype calculation driver
595 h = default_h
    (x, sdx, y, sdy, cor) = np.transpose(data)

```



```

n = data.shape[0]
today = datetime.datetime.now();
pr("=====\n"+ \
600     "running spine.py on "+today.ctime())
res = huber2(data)
if res[0] != 0:
    print("sample "+title+" not calculated")
    return "bad"
605 (a, b) = theta = res[1]
ucovtheta = res[2]
(age, sdage) = calcage(theta, ucovtheta)
e = a + b * x - y
sde = np.sqrt(b**2 * sdx**2 - 2 * b * sdx * sdy * cor + sdy**2)
610 r = e/sde
s = nmad(r); slim = 1.92 - 0.162 * np.log(10 + n);
if s < slim:
    pr(("sample "+title+": s = %0.2f"+ ": isochron " + "age = %0.3f +/- %0.3f Ma") % \
        (s, age, 1.96 * sdage), printto = where)
615 else:
    pr(("sample "+title+": s = %0.2f"+ ": errorchron " + "age = %0.3f Ma") % \
        (s, age), printto = where)
return [0, age, sdage, theta]

620 # -----

# data rows: x sdx y sdy cor
data = np.loadtxt("data0708.txt", delimiter=",")

625 recipe("0708", data, where=standard); print()

```

Datafile for sample 0708, data0708.txt, see Fig. 6

```

73.2064, 1.12543, 0.753, 0.0075, -0.068224
260.417, 4.06901, 0.435, 0.01, 0.18853
169.205, 2.43357, 0.577, 0.01, 0.45644
630 79.1766, 0.908995, 0.751, 0.01, 0.19585
212.766, 2.94251, 0.473, 0.0085, 0.37494
154.56, 1.79165, 0.615, 0.0105, 0.22567
217.391, 2.83554, 0.474, 0.0095, 0.27879
209.644, 4.83455, 0.484, 0.011, 0.10969
635 144.092, 2.49151, 0.647, 0.0105, 0.10222
174.216, 1.97283, 0.584, 0.009, 0.21416
224.215, 3.26771, 0.477, 0.012, 0.26464
236.407, 3.35329, 0.461, 0.0115, 0.14718
161.551, 2.87086, 0.628, 0.011, -0.041164

```

```

640 265.252, 5.62869, 0.385, 0.0115, -0.043072
    152.439, 2.32377, 0.608, 0.0095, 0.019543
    151.745, 2.30266, 0.626, 0.0105, 0.0030752
    101.112, 1.17572, 0.727, 0.0085, 0.038467
    265.182, 3.41058, 0.427, 0.0095, 0.070384
645 286.78, 3.16634, 0.391, 0.0085, 0.24059
    287.604, 3.5568, 0.365, 0.008, -0.041298
    264.69, 2.83747, 0.419, 0.008, 0.15939
    274.574, 2.67638, 0.378, 0.008, 0.17686
    212.314, 4.28235, 0.501, 0.013, 0.34121
650 161.29, 1.69095, 0.591, 0.009, 0.14398
    140.647, 1.58253, 0.633, 0.0105, 0.18753
    183.15, 2.18036, 0.557, 0.0105, 0.49436
    218.818, 2.39407, 0.53, 0.012, 0.21725
    312.5, 5.3711, 0.334, 0.01, -0.080507
655 227.79, 2.20526, 0.49, 0.0105, 0.073412
    212.766, 2.71616, 0.507, 0.011, 0.25544
    139.276, 2.03676, 0.652, 0.01, 0.44912
    179.533, 2.25625, 0.556, 0.0105, 0.24303
    224.215, 2.51362, 0.48, 0.0085, 0.11165
660 219.78, 3.62275, 0.519, 0.0115, 0.31258
    165.017, 2.8592, 0.59, 0.0115, 0.03575
    145.773, 2.33746, 0.61, 0.0105, 0.098985
    239.808, 4.02556, 0.442, 0.0095, -0.10478
    187.266, 2.80548, 0.538, 0.0125, 0.11864
665 255.232, 2.63831, 0.443, 0.0085, 0.025538
    141.443, 4.10124, 0.616, 0.011, -0.15512
    115.34, 0.997753, 0.707, 0.01, 0.15087
    117.509, 1.17371, 0.68, 0.008, 0.33891
    73.6377, 0.623589, 0.757, 0.0065, 0.57883
670 160.256, 2.31139, 0.605, 0.012, 0.16382
    149.701, 1.56872, 0.619, 0.009, 0.24589
    245.278, 2.58694, 0.452, 0.008, 0.33748
    251.256, 4.10343, 0.435, 0.014, 0.3589
    130.208, 2.11928, 0.666, 0.011, 0.18376
675 276.243, 4.19706, 0.419, 0.01, 0.16668
    298.508, 4.90087, 0.359, 0.0105, -0.090909
    381.679, 6.40989, 0.241, 0.013, 0.0073965

```

### Example output, running on the command line

```
running spine.py on Mon Sep 14 14:10:55 2020
```

```
680 sample 0708: s = 1.24: isochron age = 13.685 +/- 0.257 Ma
```

## Appendix D: Simulation setup

This work was originally motivated by the dating of speleothems using the lower intercept with a U-Pb Concordia in Tera-Wasserburg style plots (Woodhead et al., 2012). This paper therefore discusses  $\{x, y\}$  data with the expectation that  $x = {}^{238}\text{U}/{}^{206}\text{Pb}$  and  $y = {}^{207}\text{Pb}/{}^{206}\text{Pb}$ , but the logic and the algorithm are in no way restricted to this system.

685 10,000 simulated datasets, each containing 5, 6, 8, 10 and 15 datapoints, respectively, were used to assess SPINE. Each dataset corresponds to an age of 4 Ma, with an underlying trend chosen to be  $y = 0.811 - 0.000474737x$ . For each dataset, the  $x$ -values were drawn from a uniform probability distribution with bounds,  $\{400, 1100\}$  (so the  $x$  are not equi-spaced). Datapoints are assigned uncertainty with  $\sigma_{x_k} = 0$  and a fixed  $\sigma_{y_k} = 0.00125$ , the latter representing the analytical uncertainty, propagated from both the  $x$  and  $y$  measurement into  $y$ . In a real  $\{{}^{238}\text{U}/{}^{206}\text{Pb}, {}^{207}\text{Pb}/{}^{206}\text{Pb}\}$  dataset,  $\sigma_{x_k}$  and  $\sigma_{y_k}$  would be  
690 finite and correlated. However, this makes no difference to the calculations once data are processed into  $r_k$  form as in Fig. 2. For a given dataset, scatter is introduced into the data by drawing the  $y$  values from an uncertainty distribution, centred on the underlying trend, that may be either Gaussian (N) or one of three contaminated Gaussian distributions—5%3N, 25%5N, or 10%10N—as in Powell et al. (2002). For  $n = 10$  and gaussian-distributed uncertainties, the age uncertainty obtained is approximately  $\sigma_t = 0.01$  Ma.

695 Results are presented in terms of kernel density estimates using an Epanechnikov kernel (Wand and Jones, 1995). Kernel density estimates (kde) are a way of presenting data that could otherwise be plotted as a histogram, normally normalised so that—like a probability distribution—the area under the kde curve is 1. The smoothness of the kde is controlled by a smoothing constant whose value was chosen to be just large enough for the kde to appear smooth, given that 10,000 datasets are used in each kde.

## 700 Appendix E: SPINE handling outliers

To see the consequence of outliers stemming from residuals from a contaminated Gaussian distribution, a dataset from simulations is shown in Fig. E1 and its corresponding quantile-quantile plot in Fig. E2. This simulation, with  $n = 50$  and 25%3N and a true age of 4.00 Ma, follows the approach in Appendix D, but the uncertainty on the  $y$  values is taken to be an order of magnitude larger (to be comparable with sample 0708). The shape of Fig. E2 is typical of contaminated Gaussian distributions  
705 in samples of this size, with outliers lying outside the band between the blue dashed lines. The SPINE age is 3.95 Ma, whilst the YORK age is higher, 4.11 Ma,  $\Delta = +3.0\sigma$  of the SPINE age, due to the effect of the outliers.  $M_{\text{swd}} = 4.35$ , so ISOPLOT would give a model 2 age, 4.19 Ma, with  $\Delta = 4.27$ , being more affected by the outliers than YORK.

In general, with larger contaminated-Gaussian datasets, the difference between the SPINE and YORK ages are not dramatic, even if there are obvious outliers in the quantile-quantile plots. In 10,000 simulated datasets with  $n = 50$  and 25%3N, a 95%  
710 confidence interval on  $\Delta$  is  $\pm 1.5$ .

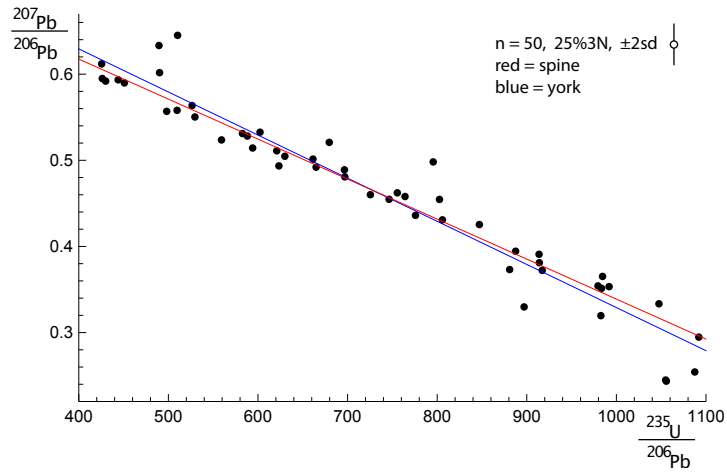


**Figure E1.** A 25%3N simulation with  $n = 50$ , with the SPINE fit in red, the YORK fit in blue. The  $2\sigma$  uncertainty applied to the  $y$  value of each datapoint is indicated in the top right of the figure. See text.

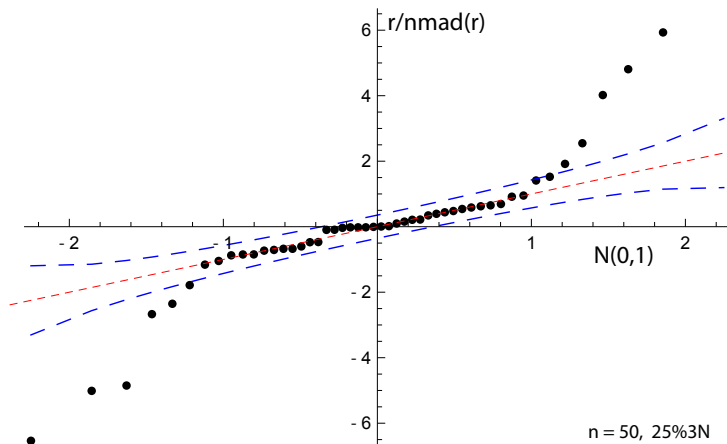


**Figure E2.** Quantile-quantile plot for example in Fig. E1. See text.

*Author contributions.* Roger Powell created the approach and coded the Python script; Eleanor Green helped validate the maths/statistics and write the paper; Tephy Marillo Sialer helped with the simulations; and Jon Woodhead oversaw the applicability of the approach.

*Competing interests.* The authors declare that they have no conflict of interest.

*Acknowledgements.* We would like to thank the anonymous reviewers for their work, particularly reviewer 4 (times two). Tim Pollard has  
715 materially helped in our understanding of the ISOPLOT code functionality. JW is funded by Australian Research Council grant FL160100028.

## References

- Brooks, C., Hart, S.R., and Wendt, I.: Realistic use of two-error regression treatments as applied to Rubidium-Strontium data. *Reviews of Geophysics and Space Physics*, 10, 551-577, 1972.
- Dickin, A.P.: Radiogenic isotope geology. Cambridge University Press, 492pp, 2005.
- 720 Fox, J.: Applied regression analysis & Generalised linear models. 3rd ed. Sage, Los Angeles, 791pp: 2016.
- Fuller, W.A.: Measurement error models. John Wiley and Sons, 440pp: 1987.
- Hampel, F.R., Rousseeuw, P.J., Ronchetti, E.M., and Stahel, W.A.: Robust statistics. Wiley and Sons, New York, 502pp, 1986.
- Huber, P.J.: Robust Statistics, John Wiley and Sons, Inc., New York: 305pp, 1981.
- Huber, P.J., and Ronchetti, E.M.: Robust Statistics, John Wiley and Sons, Inc., New York: 354pp, 2009.
- 725 Ludwig, K. R.: Isoplot/Ex Version 3.75: A Geochronological Toolkit for Microsoft Excel. Special Publication 4, Berkeley Geochronology Center, 75pp, 2012.
- Maronna, R.A., Martin, D., Yohai, V.J. and Salibián-Barrera, M.: Robust statistics. John Wiley and Sons, Chichester, 430pp, 2019.
- McLean, N.M.: Straight line regression through data with correlated uncertainties in two or more dimensions. *Geochimica et Cosmochimica Acta*, 124, 237–249, 2014.
- 730 Powell, R., Woodhead, J., and Hergt, J.: Improving isochron calculations with robust statistics and the bootstrap. *Chemical Geology* 185, 191–204, 2002.
- Reiners, P.W., Carlson, R.W., Renne, P.R., Cooper, K.M., Granger, D.E., McLean, N.M., Schoene, B.: *Geochronology and Thermochronology*. John Wiley & Sons, 464pp, 2018.
- Siegel, A.F.: Robust regression Using repeated medians. *Biometrika*, 69, 242–244, 1982.
- 735 Titterton, D.M., and Halliday, A.N.: On the fitting of parallel isochrons and the method of least squares. *Chemical Geology*, 26, 183–195, 1979.
- Tukey, J.W.: A survey of sampling from contaminated distributions, in: *Contributions to Probability and Statistics*, I. Olkin, Ed., Stanford University Press, 1960.
- Vermeesch, P.: IsoplotR: a free and open toolbox for geochronology. *Geoscience Frontiers*, 9, 1479–1493, 2018.
- 740 Wand, M.P. and Jones, M.C.: Kernel smoothing. Chapman and Hall, London. 212pp, 1995.
- Wendt, I., and Carl, C.: The statistical distribution of the mean squared weighted deviation. *Chemical Geology (Isotope Geosciences Section)* 86, 275–285, 1991.
- Woodhead, J., Hand, S.J., Archer, M., Graham, I., Sniderman, K., Arena, D.A., Black, K.H., Godhelp, H., and Price, E.: Developing a radiometrically-dated chronologic sequence for Neogene biotic change in Australia, from the Riversleigh World Heritage Area of Queensland. *Gondwana Research* 29, 153–167, 2016.
- 745 Woodhead, J., Hellstrom, J., Pickering, R., Drysdale, R., Paul, B., and Bajo, P.: U and Pb variability in older speleothems and strategies for their chronology. *Quaternary Geochronology* 14, 105–113, 2012.
- Woodhead, J. and Petrus, J., Exploring the advantages and limitations of in situ U-Pb carbonate geochronology using speleothems, *Geochronology* 1, 67–84,
- 750 <https://doi.org/10.5194/gchron-1-69-2019>.
- York, D.: Least squares fitting of a straight line. *Canadian Journal of Physics*, 44, 1079–1086: 1966
- York, D.: Least squares fitting of a straight line with correlated errors. *Earth and Planetary Science Letters* 5, 320–324, 1969.

York, D., Evensen, N.M., Martinez, M.L., and Delgado, J.D.: Unified equations for the slope, intercept, and standard errors of the best straight line. *American Journal of Physics* 72, 367–375, 2004.